HTML ABSTRACT + LINKS

JOURNAL OF CHEMICAL PHYSICS VOLUME 121, NUMBER 21 1 DECEMBER 2004

HREELS, STM, and STS study of CH_3-terminated Si(111)-(1×1) surface

Taro Yamada[a)]
The Institute for Chemical and Physical Research (RIKEN), 2-1 Hirosawa, Wako-shi, Saitama 351-0198, Japan and Center for Interdisciplinary Research, Tohoku University, 6-3 Aramaki-aza-Aoba, Aoba-ku, Sendai 980-8578, Japan

Maki Kawai
The Institute for Chemical and Physical Research (RIKEN), 2-1 Hirosawa, Wako-shi, Saitama 351-0198, Japan and Department of Advanced Materials Science, Graduate School of Frontier Sciences, The University of Tokyo, Kashiwa, Chiba 277-8561, Japan

Andrzej Wawro
Center for Interdisciplinary Research, Tohoku University, 6-3 Aramaki-aza-Aoba, Aoba-ku, Sendai 980-8578, Japan and Institute of Physics, Polish Academy of Sciences, Al. Lotnikow 32/46, 02-668 Warsaw, Poland

Shozo Suto
Department of Physics, Graduate School of Science, Tohoku University, 6-3 Aramaki-aza-Aoba, Aoba-ku, Sendai 980-8578, Japan

Atsuo Kasuya
Center for Interdisciplinary Research, Tohoku University, 6-3 Aramaki-aza-Aoba, Aoba-ku, Sendai 980-8578, Japan

(Received 25 May 2004; accepted 27 August 2004)

An ideally (1×1)-CH_3(methyl)-terminated Si(111) surface was composed by Grignard reaction of photochlorinated Si(111) and the surface structure was for the first time confirmed by Auger electron spectroscopy, low energy electron diffraction, high-resolution electron energy loss spectroscopy (HREELS), scanning tunneling microscopy (STM), and scanning tunneling spectroscopy (STS). HREELS revealed the vibration modes associated to the CH_3-group as well as the C-Si bond. STM discerned an adlattice with (1×1) periodicity on Si(111) composed of protrusions with internal features, covering all surface terraces. The surface structure was confirmed to be stable at temperatures below 600 K. STS showed that an occupied-state band exists at gap voltage of −1.57 eV, generated by the surface CH_3 adlattice. This CH_3:Si(111)-(1×1) adlayer with high stability and unique electronic property is prospective for applications such as nanoscale lithography and advanced electrochemistry. © *2004 American Institute of Physics.* [DOI: 10.1063/1.1808121]

I. INTRODUCTION

Monolayers of organic adsorbates on silicon wafer surfaces have prospective properties for applications in nanometer-scale industrial technology.[1,2] Organic moieties covalently bonded to surface Si atoms are utilized in exploring advanced processes of nanofabrication.[3–11] Expected applications are not only for controlling the reactivity of Si surfaces in nanometer-scale lithography[3–6] but also for connecting polymers such as DNA and proteins to Si surfaces for purposes of bioassay.[7–11]

Within the diversity of organic species, alkyl (C_nH_{2n+1}-type hydrocarbon moieties) monolayers directly bonded on silicon surfaces are structurally simple and have useful properties for nanofabrication.[3–6] The ultimate thinness and chemical robustness of alkyl monolayers are promising in applications in high-resolution lithography of the future generation. The method of electron-beam patterning of alkyl monolayers was actually explored.[4–6] The alkyl adsorbates were demonstrated to act as a robust resist layer. The alkyl monolayers can survive in a plating solution containing powerful chemicals such as HF for a period to deposit a visibly thick metal layer on the electron-bombarded portions.[5] Micropatterning on alkyl monolayers by electrolytic oxidation was also recently examined.[12] Because of the ultimate thinness and this chemical robustness, the alkyl monolayers can be applied for nanoscale patterning of the future generation.

In regard of such application demands, it is important to establish the processes to deposit desired organic moieties covalently bonded to Si surface. The direct deposition of hydrocarbons on Si flat surfaces was first reported by Chidsey and co-workers,[13] in which terminally-double-bonded linear olefins were adsorbed on hydrogen-terminated Si surfaces under ultraviolet irradiation. This type of photoreactions has been recently applied for practical exploitations.[14] Thermal reaction of olefins in liquid phase was also proposed for convenience.[15,16] Due to conventional reaction conditions, those methods tend to introduce SiO_2 deposits detected by x-ray photoelectron spectroscopy.[13,17] For applications in electronic devices and electrochemistry,

a)Author to whom correspondence should be addressed. Fax: +81-48-462-4663.

 © 2004 American Institute of Physics

Downloaded 22 Aug 2012 to 131.215.16.11. Redistribution subject to AIP license or copyright; see http://jcp.aip.org/about/rights_and_permissions

oxygen-free surfaces of modified Si are required to avoid inhomogeneous material distribution and unexpected insulation. Another route of alkyl deposition by Grignard reagent [C_xH_yMgCl (or Br, I)] was proposed by Bansal *et al.*,[18,19] who performed chlorination of H:Si(111) by PCl_5 before Grignard reaction. Later, Boukherroub *et al.*[20] reported that even H:Si(111) can react with long-chain alkyl Grignard reagents, forming robust, hydrophobic Si surfaces.

Yamada *et al.* found that the terminating hydrogen atoms on the reacting H:Si(111)-(1×1) can be *partially* replaced with CH_3 groups by contact with CH_3MgBr.[21] The adlayer was a mixture of CH_3- and leftover H- occupying the surface Si sites randomly.[4] High-resolution electron energy loss spectroscopy HREELS showed that the CH_3 groups on Si(111) are covalently bonded to the topmost Si atoms.[21] Fidélis *et al.* conducted electrolysis on H:Si(111) in a solution of Grignard reagent, and claimed 100% methylation of Si(111) on the basis of loss of the H–Si stretching signal in surface infrared spectroscopy.[22] We realized that a small leftover amount of terminating H–Si is detectable by HREELS (Ref. 21) but occasionally undetectable by infrared reflection absorption.[4] On porous silicon substrates, vibrational identification of adsorbed methyl groups is more complicated as the substrate surfaces are not homogeneous and some different types of CH_3 might coexist.[23,24] Impurity assessment is not easy, either. It is obviously more rational to use a flat, well-defined single crystalline substrate in order to establish chemistry of organic deposition of the modern standard.

Chlorine-terminated Si(111) is anticipated to have better reactivity for complete methylation of Si(111) upon Grignard deposition.[17–19,25] Webb and Lewis discussed on several synthetic routes to deposit CH_3 on Si(111), involving chlorination of Si.[17] The Cl:Si(111) surface was reported to possess a good two-dimensional periodicity of (1×1) (Ref. 26) and exhibits a Cl–Si stretching vibration mode at 587 cm^{-1}.[27] The ultraviolet photoassisted gas-surface chlorination of Si(111) seems to etch away the outermost layers of Si, and the renewed surface seems to be always fresh Cl:Si(111)-(1×1) without major contamination. Cl:Si(111) seems to react slowly with components of air and thus handling in vacuum or in inert gas is necessary.[27,28]

In this paper, we present a complete set of structural information on CH_3 groups deposited by Grignard reaction on chlorine-terminated Cl:Si(111), taking after a part of the preliminary scanning tunnel microscopy (STM) and electrochemical observations.[28] The surface was carefully prepared and investigated by low energy electron diffraction (LEED) to see the homogeneity of surface, Auger electron microscopy (AES) to assess the purity of adlayer, HREELS to clarify the bonding between the composing atoms, by STM to confirm the (1×1) periodicity, and by scanning tunneling spectroscopy (STS) to address the electronic property. The (1×1) periodicity of Cl:Si(111) is considered to be inherited after treatment in Grignard reagent to form a methyl (1×1) adlattice. We furthermore attempted to discern the internal structure of features of CH_3 groups by STM.

II. EXPERIMENT

The present process of depositing CH_3 group on Si(111) is schematized as follows:

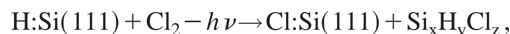

$$\mathrm{H{:}Si(111)} + \mathrm{Cl_2} - h\nu \rightarrow \mathrm{Cl{:}Si(111)} + \mathrm{Si_xH_yCl_z},$$

$$\mathrm{Cl{:}Si(111)} + \mathrm{CH_3MgBr} \rightarrow \mathrm{CH_3{:}Si(111)} + \mathrm{Mg(Cl,Br)_2}.$$

The sample chips (30 mm×11 mm) diced from commercial *n*-Si(111) wafers (Shinetsu Handotai Co., Ltd., single-side polished, thickness=0.6 mm, resistivity =3−8 Ω cm) were washed in trichloroethylene and acetone and immersed in a SPM solution (sulfuric acid–hydrogen peroxide mixture, three parts of concentrated H_2SO_4+one part of 30% H_2O_2 at 120 °C) for 10 min to form a thin oxide protective layer on Si(111), designated as O/Si(111). The O/Si(111) specimens were immersed in pure H_2O for storage. Just before use, the O/Si(111) was thoroughly dried by blowing He gas and then immersed in 40% NH_4F solution for 10 min to remove the surface oxide. Upon taking the chip out of the solution, the surface was strongly hydrophobic and almost automatically dried itself. This is the method employed to prepare H:Si(111)-(1×1).[29]

The dried H:Si(111) was placed in a 20 ml Pyrex Schlenk tube for chlorination and Grignard reaction. The Schlenk tube was connected to a vertical water-cooled reflux condenser linked to a liquid paraffin bubbler. One of the two entrances on the valve of Schlenk tube was connected to an Ar cylinder (Nihon Sanso, impurity level $<10^{-6}$), and the other was stopped by a rubber septum for reagent injection. The Schlenk tube containing the Si wafer was purged at an Ar flow rate of 10 l h^{-1} for at least 20 min to achieve dry O_2-free environment.

In order to chlorinate H:Si(111), we started to irradiate UV light at the polished side of Si wafer through the Pyrex wall from a high-pressure mercury lamp (100 W, Sen Engineering Co., Ltd., Japan), and then started introducing 1% Cl_2 gas diluted in Ar from a commercial cylinder (Nihon Sanso, Japan) through a syringe needle punched into the septum. 1% Cl_2/Ar was continuously introduced at 1 atm and bubbled out for 4–5 min. A perfect Cl:Si(111)-(1×1) was supposed to be formed in this step. A commercial solution of CH_3MgBr in tetrahydrofuran (THF) at 0.8*M*–1.0*M* (Kanto Chemicals, Japan) was then immediately pumped in through a syringe needle. The purge gas was switched to pure Ar, and the Schlenk tube was heated in an oil bath at 60 °C for 5–6 h. This temperature was determined to accelerate the reaction but not to boil the solvent.

To terminate the Grignard reaction, the Si wafer was removed from the Schlenk tube into air, and rinsed briefly in THF added with 1 % w/w CF_3COOH to remove greasy leftover reagent. Then the surface was rinsed with pure H_2O, dried, and washed in 1,1,2-trichloroethane by an ultrasonic cleaner for 2–5 min. The specimen was sliced to adjust to the sample carrier and mounted on it for HREELS/LEED or STM/STS measurement. The methylated specimens were stored in vacuum for the following measurement. HREELS was performed by an ultrahigh vacuum (UHV) apparatus equipped with an Ibach-type spectrometer (SPECS, Germany) and a rear-view LEED optics (Omicron, Germany). Another UHV apparatus was used for a variable-temperature

Downloaded 22 Aug 2012 to 131.215.16.11. Redistribution subject to AIP license or copyright; see http://jcp.aip.org/about/rights_and_permissions

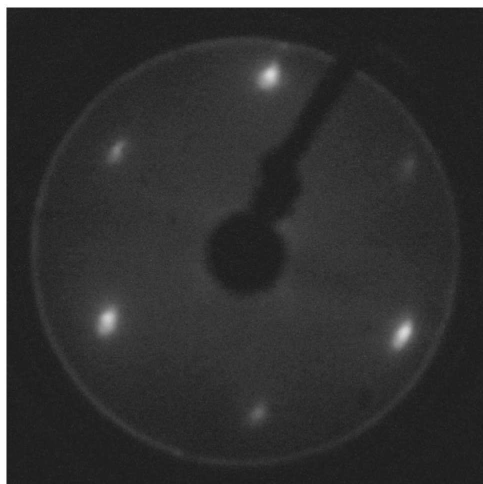

FIG. 1. LEED pattern of the methylated Si(111) surface. The sample was prepared by (1) chlorination in 1 atm 1% Cl_2/Ar under UV irradiation for 5 min, (2) Grignard reaction in 0.93*M* CH_3 MgBr in THF at 60 °C for 324 min, (3) rinsing in 1% w/w CF_3COOH in THF, ultrapure water, and 1,1,2-trychloroethane, and (4) dried in air. Incident electron energy = 42.3 eV.

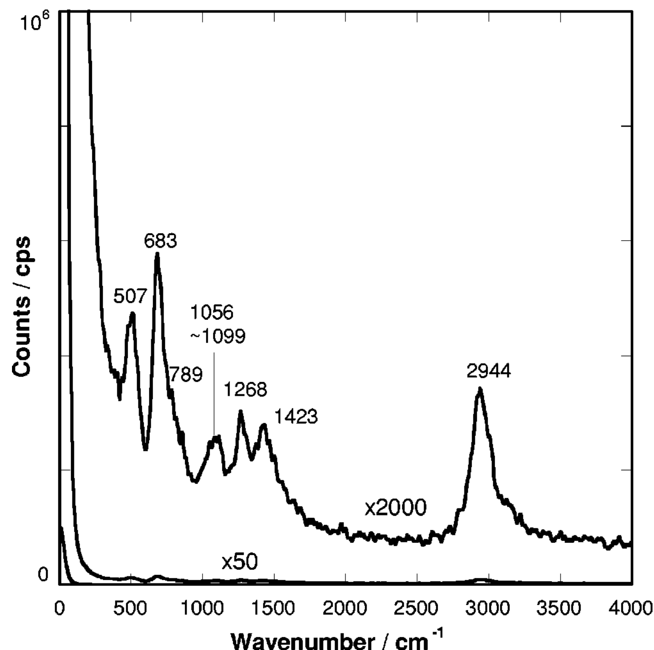

FIG. 2. HREELS of the methylated Si(111) surface. The same sample as that of Fig. 1 was used. HREELS incident electron energy = 2.84 eV, incident angle = exit angle = 60° from the surface normal. The full width at half maximum of inelastic peak = 7.6 meV.

STM setup (Omicron, Germany). Additionally, Auger electron spectroscopy (AES) was performed by a cylindrical mirror analyzer (CMA) integrated with a coaxial electron gun (CMA-2002, Kitano Seiki, Japan) equipped in a separate UHV chamber.

We paid attention to maintain a good vacuum in the sample introductory system so as not to contaminate the sample during transferring. Each of the analysis chambers was equipped with a two-stage introductory system from air to UHV. The stages are small chambers serially connected with gate valves. Each of the small chambers was pumped independently by a turbomolecular pump. The loading chamber from air was additionally connected to a liquid-nitrogen cooled sorption pump. This sorption pump was used for pumping from the atmospheric pressure to $\sim 10^{-3}$ Torr and switched to the turbomolecular pump running at the top speed. This procedure realizes oil-free evacuation and eliminates the chance of contamination by hydrocarbons.

III. RESULTS AND DISCUSSION

A. AES, LEED, and HREELS observations

AES (incident electron energy = 2.0 keV, first-derivative spectrum) was performed for some pieces of Si(111) deposited with CH_3– by the method described above. No signals for Cl (LMM transition, 185 eV), Br (MNN, 1400 eV), and Mg (LMM, 58 eV) were detected. The lower detection limit of the CMA setup was ~1% for Br and was lower than 1% for Cl and Mg. These elements mediating Grignard reaction were negligible as components of the completed surface structure. Oxygen signal (KLL, 510 eV) was also below the detection limit (<0.5%).

Figure 1 shows a LEED photograph (incident electron energy = 42.3 eV) of methylated surface. A pattern composed of sharp spots in a hexagonal arrangement is seen. The lattice constant of this hexagonal unit cell is estimated to be ~0.4 nm by examining the spot positions and the geometrical arrangement of LEED optics. This value indicates that the adlattice periodicity of the methylated surface was the same as that of Si(111)-(1×1) = 0.38 nm. The sharpness of LEED pattern with a dark background backs up for (1×1) arrangement of CH_3– groups, however, it is difficult to extract the contribution of (1×1) superlattice from the same substrate (1×1) pattern. STM observation is indispensable to determine the arrangement of CH_3– groups.

HREELS measurement for several pieces of methylated surface reproducibly yielded spectra as shown in Fig. 2. The positions of vibration signals are nearly the same as those found on H:Si(111) treated in CH_3MgBr/THF.[21] The frequencies were assigned to the vibration modes by referring to the infrared spectra of methyl silanes[30–33] as well as HREELS of a hydrocarbon adsorbate on Si.[34] The peaks in Fig. 2 are assigned as following: 2944 cm^{-1} = C–H asymmetric and symmetric stretching (due to the resolution limitation, these two modes are merged), 1423 cm^{-1} = C–H asymmetric bending, 1268 cm^{-1} = symmetric bending, 1056–1099 cm^{-1} = SiO_2 impurity, 789 cm^{-1} = CH_3 rocking, 683 cm^{-1} = C–Si stretching, and 507 cm^{-1} = C–Si bending.

The amount of SiO_2 impurity converted from the intensity of loss peak, according to the process of estimation described previously,[21] does not exceed 0.1% of the surface. This content of SiO_2 is likely to be formed during the Grignard reaction of a trace amount of air mixed in the purging gas. No signals for H–Si stretching (~2080 cm^{-1}) and Cl–Si stretching (~590 cm^{-1}) were found in the present case. CH_3– was the only one dominant species that terminates the Si surface.

The vibration signal at 683 cm^{-1} confirms that a CH_3– moiety is fixed on a surface Si atom by a covalent single bond. Taking into account the sp^3 valence geometry

Downloaded 22 Aug 2012 to 131.215.16.11. Redistribution subject to AIP license or copyright; see http://jcp.aip.org/about/rights_and_permissions

of CH_3- groups and Si atoms in the crystal, we can conclude that the C–Si bonds are vertical to the surface plane, and that the CH_3- groups are placed on the on-top sites with the H atoms protruding from the surface.

It is interesting to address the rotation of CH_3- group around the C–Si axis with respect to the substrate.[35] The rotation of CH_3- on Si(111) can be analogized from the torsion and internal rotation of C–Si bond in an isolated CH_3SiH_3 (methylsilane) molecule, whose single excitation energy is 200 cm^{-1} and barrier for rotation is 590.5 cm^{-1}.[36] The peaks corresponding to this torsion and the overtones are not recognized in Fig. 2.

In the case CH_3SiH_3 molecule, the rotational ground-state molecules are dominant at room temperature and the angle of rotation stays near the equilibrium position. On the other hand, a CH_3 group on Si(111) is incorporated in a dense adlayer and the excitation of CH_3- rotation must be influenced by interaction with the substrate solid Si and might be also with other CH_3- groups in the neighborhood. The rotational barrier of CH_3 on Si(111) is anticipated to be higher than that of isolated CH_3SiH_3, and the absence of corresponding HREELS peak might be because of the low incident electron energy not suitable for collective excitation. We may approximate the motion of CH_3- group by rotational locking at the ground-state equilibrium position under the present condition.

B. STM observation

STM imaging was performed in the constant-current topographic mode at room temperature by a sharpened tungsten tip. In some cases the sample was heated up to 600 K in ultrahigh vacuum to remove volatile debris. The scale along the surface was calibrated by imaging H:Si(111)-(1×1) surface (hexagonal, lattice constant=0.38 nm). The tunneling of tip current was often unstable in the gap voltage range examined (-2 V∼$+2$ V), except in a small region near -1.5 V (sample negative). A preset tunneling current higher than 2 nA, was also usually needed to complete scanning a whole frame of high-resolution image. Imaging was impossible at positive gap voltages, examined in the range below $+2.0$ V, due insensibly small tunneling conductivity. The tunneling condition was examined by STS in detail later.

Figure 3 shows a wide-range STM image recorded on the methylated surface. The surface consisted of flat wide terraces separated by step lines that are composed of step edges parallel to the [11$-$2] and equivalent directions. This step-and-terrace feature is similar to that of H:Si(111)-(1×1) with holes attached to the step edges. The largest size of those holes was some tens of nanometers in diameter, and the depths matched one of the integral multiples of the monoatomic step height of Si(111)=0.31 nm. The bottoms of holes are considered to be the same methylated patches as those on the terraces. The distribution of holes depended on the procedure of introducing Cl_2/Ar gas and starting UV irradiation in the chlorination step. The number of holes could be increased or decreased by varying the condition of UV photochlorination of H:Si(111).

By zooming into a flat terrace, arrays of molecular features were discerned. Figure 4 summarizes a series of images of methylated Si(111) obtained by various STM tips. Figure 4(a) shows a well-ordered lattice of protrusions spreading in an area of 10 nm square. The methylated surface exhibited hexagonal symmetry with the lattice constant measured to be ∼0.4 nm, equal to that of Si(111)=0.384 nm. STM images of H:Si(111) were recorded for reference and used for X, Y, and Z scale calibration. Figure 4(b) shows one of the H:Si(111) images. Compared to methylated Si(111), H:Si(111) could be stably imaged with a low tunneling current below 1 nA. To detect a significant corrugation on methylated Si(111), the tip had to be kept near the surface by raising the preset tunneling current.

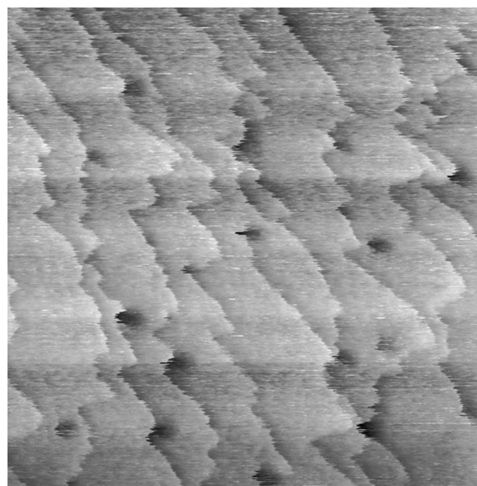

FIG. 3. A wide-range STM image of methylated Si(111). The same sample as that of Fig. 1 was used. Scan size=500 nm×500 nm (512×512 pixels), gap voltage=-1.21 V (sample negative), preset tunneling current=2.58 nA.

The lattice images of small frames, shown in Figs. 4(c)–4(f) are distorted due to the thermal drift of STM setup, and the distances in the images are not accurately scaled. However, in most of the high-resolution images obtained on methylated Si(111), the internal structures of arrayed protrusions are distinguishable.

The protrusions in Fig. 4(c) are shaped triangular, and those in Fig. 4(d) are filled circles. These two images were recorded at the same gap voltage (-1.16 V) but at different preset currents. It was difficult to reproduce images with similar protrusion shapes just by controlling the tunneling condition. The apparent shape of protrusion seems to depend on the modification of tip apex surface, which is usually uncontrollable. However, at gap voltages near -1.1 V, the protrusions always looked filled, namely, no holes were recognized at the centers of protrusions.

At gap voltages near -1.5 V, the images [Figs. 4(e) and 4(f)] consist of arrayed rings, namely, there is a hole at the center of each protrusion. The density grayscale along the bar of each ring is not homogeneous, and the rings sometimes look slightly tilted. This kind of ring-shaped protrusion was reproducibly observed around this gap voltage.

These internal structures are distributed within a unit cell with a lattice constant of ∼0.4 nm, and to look into the features of this scale is a challenge by STM. This sort of

Downloaded 22 Aug 2012 to 131.215.16.11. Redistribution subject to AIP license or copyright; see http://jcp.aip.org/about/rights_and_permissions

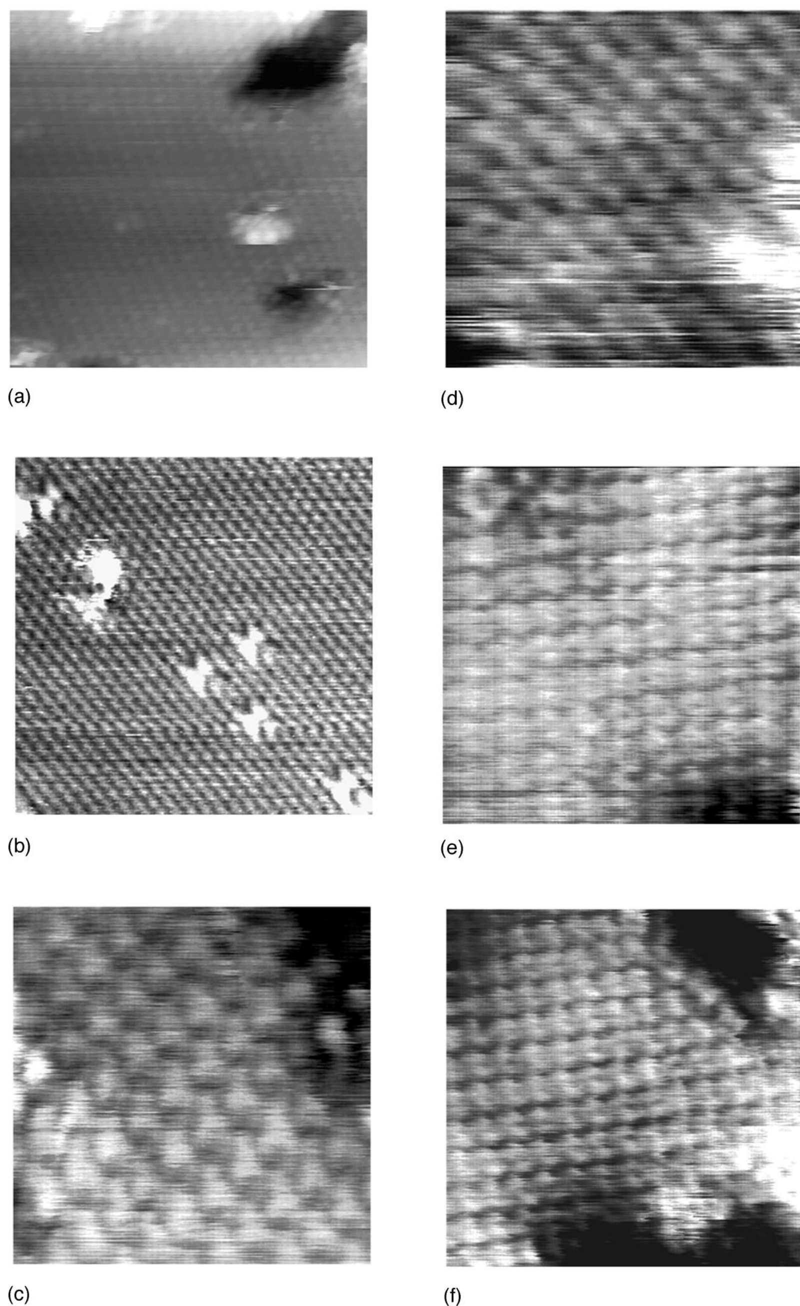

FIG. 4. High-resolution STM images of the methylated Si(111). (a) Scan size = 10 nm × 10 nm, gap voltage = −1.48 V (sample negative), preset tunneling current = 2.38 nA; (b) An image of H:Si(111)(1×1) for reference. 10 nm×10 nm, −1.03 V, 0.56 nA; (c) 4 nm ×4 nm, −1.16 V, 7.12 nA; (d) 4 nm×4 nm, −1.16 V, 2.48 nA; (e) 4 nm×4 nm, −1.51 V, 19.65 nA; (f) 5 nm×5 nm, −1.51 V, 7.88 nA.

internal structure was never observed on H:Si(111) in our own operation. The protrusions on H:Si(111) were always round spots. The arrayed features in methylated surface were certainly different from those on H:Si(111).

By annealing up to 600 K in UHV, the wide-range feature, the microscopic arrangement of protrusions, and the internal structure of protrusions exhibited no significant change in STM images. CH_3:Si(111)-(1×1) is thermally stable for temperatures below 600 K in vacuum.

We take the surface electronic orbitals into account to interpret the shapes of protrusions in the STM images, roughly classified into the two categories: filled/triangular spots and rings. The triangular protrusions in Fig. 4(c) are considered to involve the shape of electronic orbital at −1.16 V. It seems that in Fig. 4(c) a higher resolution was occasionally achieved than in Fig. 4(d) by modification of the tip surface. This shape observed at gap voltage = −1.16 V is not embodied by the C sp^3 orbital of CH_3– moiety of which binding energy is estimated to be as high as 11 eV for CH_3SiH_3 molecule[37] or 7 eV from the Fermi level for CH_3 on Cu(110).[38] The triangular distribution is probably due to a surface electronic state generated by perturbation of the threefold symmetric Si bulk state by the CH_3– adsorbates. In this sense, the equilibrium rotational direction of CH_3– about C–Si bond does not primarily influence the consideration of observed shapes. Determination of the CH_3– equilibrium rotational angle is difficult without advanced theoretical assistance. It is natural to assume the angle between the C–H bond and the Si–Si backbond to be 60° [in the top view of Si(111)] by analogy to the equilibrium rotational position in CH_3SiH_3 molecule.[37]

Downloaded 22 Aug 2012 to 131.215.16.11. Redistribution subject to AIP license or copyright; see http://jcp.aip.org/about/rights_and_permissions

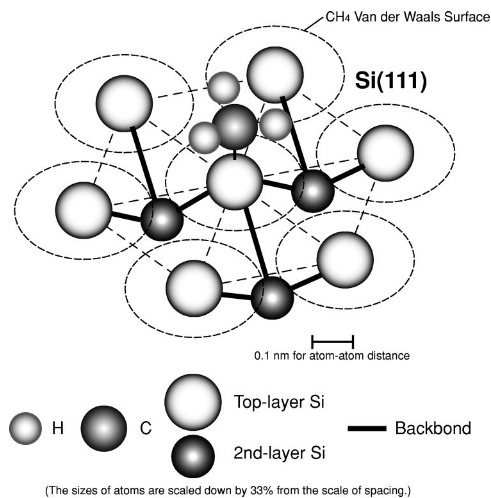

FIG. 5. The dimensions of CH_3– group attached to Si(111) taken from the molecular structures of CH_4 (Ref. 39) and CH_3SiH_3 (Ref. 40) and the van der Waals radii of element atoms (Ref. 41). (The second-layer Si atoms are placed just to indicate the directions of backbonds. These Si atoms are undersized, and their depths are exaggarated.)

The ring-shaped protrusions observed at ~ -1.5 V is also probably mainly contributed by a surface state band generated by perturbation by CH_3– adsorbates. STM imaging was relatively stable at this gap voltage by the aid of rather large tunneling conductivity.

The dimensions of CH_3– group attached on Si(111) are illustrated in Fig. 5. The bonding distances C–H = 0.11 nm and C–Si = 0.19 nm are taken from the molecular structures of CH_4 (Ref. 39) and CH_3SiH_3.[40] By using the van der Waals radius of H = 0.12 nm,[41] the outer diameter of CH_4 is estimated to be 0.34 nm. This diameter is smaller than the nearest Si–Si distance on Si(111) = 0.38 nm. The angle of CH_3– rotation about the C–Si bond is adjusted so that the angle between C–H and Si–Si backbond be 60° in the projection onto the surface plane. The relative sizes of features seen in Fig. 4 accommodated within the Si(111) unit cell reasonably match with these molecular constants. Although the internal features of periodic protrusion are not the same in image by image, they are in conformity with the geometrical structure of tetrahedral CH_3– group with the C–Si bond vertical to the basal plane. The close-packed diameter of CH_4 is estimated to be 0.41 nm from the crystallographic data of solid "Phase III" methane.[42] This size is significantly larger than the Si–Si distance on Si(111), demonstrating that this compressed arrangement of CH_3– on Si(111) is enforced by the substrate lattice.

We have doubtlessly confirmed that every outermost Si atom is terminated by one CH_3– group on Si(111) terraces, and hereafter we designate this structure as CH_3:Si(111)-(1×1). This adlayer is recognized for the first time as a well-ordered closely-packed adlattice of organic moieties bonded on Si(111) covalently. The rotation of CH_3– groups about the C–Si bonds might be interlocked in this densely-packed adlayer. It is seen in Fig. 5 that the fully (1×1)-terminating moieties other than CH_3– should be as small as CH_3– in the projection onto Si(111) plane to form a (1×1) adlattice. Possibilities are CF_3–, N≡C–, HC≡C–, and so on. CH_3–CH_2–, for example, is slightly too large to be packed into a (1×1) superlattice.

C. STS measurement

The suitable gap voltage in STM operation was limited within a narrow range near -1.5 V (sample negative) in taking images of the CH_3:Si(111)-(1×1). We performed STS to study this limitation by examining the I (the tunneling current)-V (the gap voltage) characteristics.

At each pixel in the scanned frame, the tip height was adjusted by the current feedback circuit so that the width of tunneling gap be constant at a given gap voltage. Then the feedback circuit was disrupted to maintain the tip height as adjusted. The tunneling current was measured while the gap voltage was scanned in the given range. One I-V characteristic curve was associated with every pixel. By averaging the I-V curves of pixels in an extended area in the frame, we obtained one I-V characteristic curve representing the area of averaging. This procedure does not differentiate the I-V characteristics depending on the positions within the adlattice unit cell. The entire I-V curve was reproducible when the averaging area was chosen within one single terrace strip without involving step edges.

Figure 6(a) shows a typical I-V characteristic curve on a terrace of CH_3:Si(111)-(1×1), compared with that of H:Si(111)-(1×1). The I-V curves are asymmetric and exhibit diodelike characteristics with the range of insulation spreading into the positive voltage region. To expand the weak features in the low current region and to demonstrate the density of electronic state, Fig. 6(a) was converted to Fig. 6(b) for CH_3:Si(111)-(1×1) and Fig. 6(c) for H:Si(111)-(1×1) by plotting numerically calculated first derivative dI/dV versus V.

The curve in Fig. 6(b) for CH_3:Si(111)-(1×1) involves two steep slopes rising at -0.59 V and $+0.47$ V, marking the energy band gap of bulk Si. A notable increase is observed in the negative voltage region rising from ~ -1.2 V. This uprise of tunneling current is composed of a large peak at -2.01 V and a distinct shoulder at -1.57 V. This shoulder includes the gap voltages at which the tunnel current was obtained with adequate stability. In the positive region (empty-state side), the dI/dV value is smaller by two orders of magnitude than that of the negative region (occupied-state side), indicating a low density of state.

The derivative curve of H:Si(111)-(1×1) in Fig. 6(c) contains a notable peak at -2.10 V, and dI/dV rises at lower gap voltage more gradually than on CH_3:Si(111)-(1×1). This spectrum agrees well with previously reported STS on H:Si(111) by Suto *et al.*[43]

It is useful to refer to studies by ultraviolet photoemission and inverse photoemission to assign the origin of this density-of-state distribution. The UPS by He *et al.* on H:Si(111) (Ref. 44) involved a peak away by 2 eV from the Fermi level, which was attributed to a transition from the valence band of Si bulk. The large peak at -2.01 V on CH_3:Si(111)-(1×1) and one at -2.10 V on H:Si(111)-(1×1) correspond to this bulk transition. The STS of H:Si(111)-(1×1) does not involve a peak near -1.5 V.

Downloaded 22 Aug 2012 to 131.215.16.11. Redistribution subject to AIP license or copyright; see http://jcp.aip.org/about/rights_and_permissions

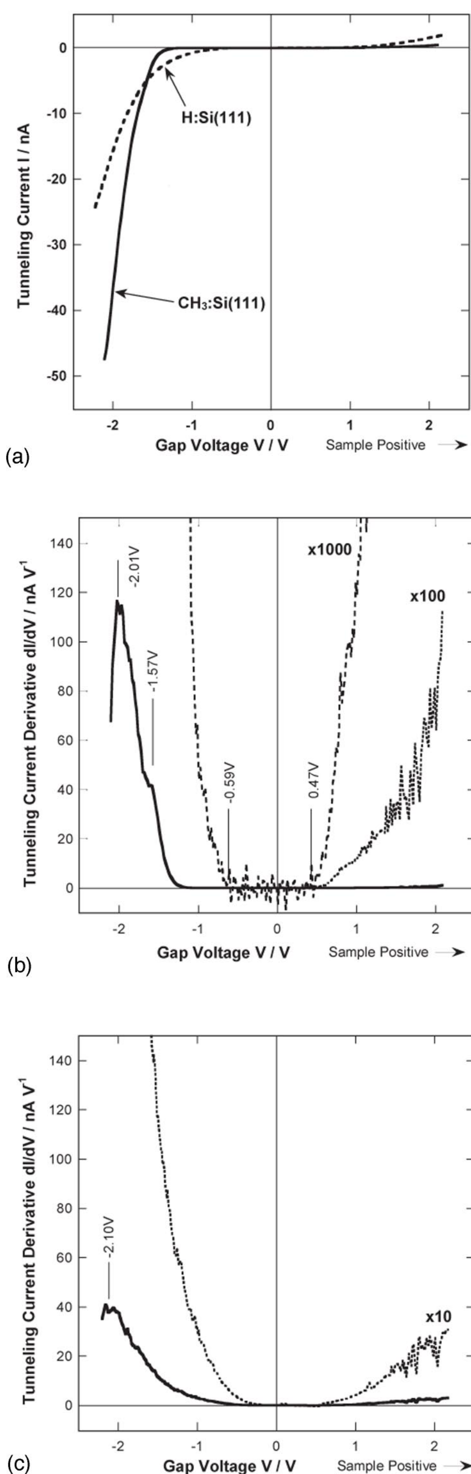

FIG. 6. Averaged STS of CH_3:Si(111)-(1×1) and H:Si(111)-(1×1) within a flat terrace. The spectra were obtained for CH_3:Si(111)-(1×1) at preset tunneling current=2.74 nA at gap voltage=−1.51 V and for H:Si(111)-(1×1) at preset tunneling current=1.14 nA at gap voltage =−1.93 V. Spectroscopic span=−2.105∼+2.105 V. The spectra was averaged for 256×256 points over an area of 4 nm×4 nm within a single terrace for each. (a) I(tunneling current) vs V(gap voltage) curves, (b) the 1st derivative dI/dV numerically calculated from the curve of CH_3:Si(111)-(1×1) in (a). The dI/dV curves multiplied by 100 and 1000 are also plotted. The negative side of ×100 curve is omitted, (c) dI/dV from the curve of H:Si(111)-(1×1) in (a). The dI/dV curve multiplied by 10 is also shown.

Evidently, the peak at −1.57 V is exclusively associated with the adlattice of CH_3- located at the outermost surface. The ring-shaped protrusions in the STM images, recorded at gap voltages near −1.5 V, are composed of the orbital of this density-of-state peak. The intensity of this peak at −1.57 V is much smaller than the bulk Si peak and it is probably appropriate to assume that this small peak is generated by perturbation of the tail of distribution of Si bulk electronic state at −2.01 V. The dI/dV value is low at gap voltages near −1.1 V that yielded features of triangular/filled protrusion. A density-of-state band as an isolated peak cannot be recognized here. STM imaging was relatively difficult due to this high gap resistance.

In the recent UPS work by Miyadera *et al.* on methylated Si(111),[45] it was shown that the Si 3p orbital contributes at the onset of their UPS near the Fermi level. The density-of-state in this region seems to the bulk Si band assigned by He *et al.*[44] No extra peak was recognized in this region of their spectra as the intensity of photoemission was too small compared to the CH_3 molecular orbital signals (binding energy=8–10 eV). The surface composition in this case might have been qualitatively different from well-ordered CH_3:Si(111)-(1×1).

It is interesting to compare the findings in Figs. 6(b) and 6(c) with the results of electrochemical I-V curve analysis by Niwa *et al.*[28] in which the electrolytic current distinctively rises at more positive potential through CH_3:Si(111) (n type) than through H:Si(111) in a $Fe(CN)_6^{3-}/Fe(CN)_6^{4-}$ redox solution.

As for the positive gap-voltage region, the inverse photoemission (IPS) studies by Bouzidi *et al.*[46,47] indicate that an unoccupied orbital of bulk Si is located at 2.6 eV from the Fermi level in the $\bar{\Gamma}$ direction. The tail of this transition peak spreads near the Fermi level. This tail region overlaps with the positive gap-voltage region in Figs. 6(b) and 6(c). The dI/dV curves certainly involve a part of rising tail in the positive gap-voltage region both on CH_3:Si(111)-(1×1) and on H:Si(111)-(1×1). The normalized tunneling conductivity $(V/I)dI/dV$ was calculated from the curve in Fig. 6(a) to compensate the difference of preset tunneling current. The value of $(V/I)dI/dV$ on CH_3:Si(111)-(1×1) is nearly constant and similar to that of H:Si(111)-(1×1) in this region. According to the IPS analysis on H:Si(111) by Bouzidi *et al.*,[46,47] no H-induced surface electronic state exists near the Si bulk state, namely, the H adlayer is transparent to electrons. Therefore, this unoccupied region below +2 V does not involve density-of-state contribution from CH_3:Si(111)-(1×1), either. The unoccupied molecular orbitals associated with the framework C–H and C–Si bonds are presumably located at higher energy level than the present gap-voltage region.

IV. CONCLUSION

The CH_3:Si(111)-(1×1) monolayer was successfully composed by photoassisted chlorination of H:Si(111) from Cl_2/Ar mixture followed by Grignard reaction in a THF solution of CH_3MgBr. HREELS resolved the vibration modes of CH_3- group and the C–Si bond, by which the co-

Downloaded 22 Aug 2012 to 131.215.16.11. Redistribution subject to AIP license or copyright; see http://jcp.aip.org/about/rights_and_permissions

valent fixation of CH_3 on every surface Si atom was confirmed. STM revealed a well-ordered (1×1) adlattice and the internal structure of adsorbed moieties. The CH_3:Si(111)-(1×1) monolayer was thermally stable up to 600 K in vacuum. STS indicated a distribution of the occupied electronic density of state at -1.57 V, generated by the CH_3 adlattice. This well-ordered CH_3:Si(111)-(1×1) with a unique electronic property is prospective in applications for nanotechnology in terms of stabilization and modification of Si wafer surface with an ultimately thin adlayer.

ACKNOWLEDGMENTS

The authors appreciate everlasting collaboration with Professor Tetsuya Osaka, Professor Takayuki Homma, and their group members Tomoyuki Inoue and Dr. Daisuke Niwa of the Department of Applied Chemistry, Waseda University (Tokyo, Japan). One of the authors (A.W.) is grateful for a support from the State Committee for Scientific Research (Poland) under the Project No. R-48.

[1] C. S. Whelan, M. J. Lercel, H. G. Craighead, K. Seshadri, and D. L. Allara, J. Vac. Sci. Technol. B **14**, 4085 (1996).
[2] H. Sugimura, K. Okiguchi, N. Nakagiri, and M. Miyashita, J. Vac. Sci. Technol. B **14**, 4140 (1996).
[3] T. Yamada, N. Takano, K. Yamada, S. Yoshitomi, T. Inoue, and T. Osaka, Electrochem. Commun. **3**, 67 (2001).
[4] T. Yamada, N. Takano, K. Yamada, S. Yoshitomi, T. Inoue, and T. Osaka, Jpn. J. Appl. Phys., Part 1 **40**, 4845 (2001).
[5] T. Yamada, N. Takano, K. Yamada, S. Yoshitomi, T. Inoue, and T. Osaka, Materials Physics and Mechanics **4**, 67 (2001).
[6] T. Yamada, N. Takano, K. Yamada, S. Yoshitomi, T. Inoue, and T. Osaka, J. Electroanal. Chem. **532**, 245 (2002).
[7] C. K. Harnett, K. M. Satyalakshmi, and H. G. Craighead, Appl. Phys. Lett. **76**, 2466 (2000).
[8] T. Livache, H. Bazin, and G. Mathis, Clin. Chim. Acta **278**, 171 (1998).
[9] R. M. Ostroff, D. Hopkins, A. B. Haeberli, W. Baouchi, and B. Polisky, Clin. Chem. **45**, 1659 (1999).
[10] R. Lenigk, M. Carles, N. Y. Ip, and N. J. Sucher, Langmuir **17**, 2497 (2001).
[11] R. Bennewitz, J. N. Crain, A. Kirakosian, J. L. Lin, J. L. McChesney, D. Y. Petrovykh, and F. J. Himpsel, Nanotechnology **13**, 499 (2002).
[12] R. Okada, T. Miyadera, T. Shimada, A. Koma, K. Ueno, and K. Saiki, Surf. Sci. **552**, 46 (2004).
[13] M. R. Linford, P. Fenter, P. M. Eisenberger, and C. E. D. Chidsey, J. Am. Chem. Soc. **117**, 2145 (1995).
[14] Z. Lin, T. Strother, W. Cai, X. Cao, L. M. Smith, and R. J. Hamers, Langmuir **18**, 788 (2002).
[15] A. B. Sieval, V. Vleeming, H. Zuilhof, and E. J. R. Sudhölter, Langmuir **15**, 8288 (1999).
[16] M. E. Quayum, T. Kondo, S. Nihonyanagi, D. Miyamoto, and K. Uosaki, Chem. Lett. **31**, 208 (2002).
[17] L. J. Webb and N. S. Lewis, J. Phys. Chem. B **107**, 5404 (2003).
[18] A. Bansal, X. L. Li, I. Lauermann, N. S. Lewis, S. I. Yi, and W. H. Weinberg, J. Am. Chem. Soc. **118**, 7225 (1996).
[19] A. Bansal, X. Li, S.-I. Yi, W. H. Weinberg, and N. S. Lewis, J. Phys. Chem. B **105**, 10266 (2001).
[20] R. Boukherroub, S. Morin, F. Bensebaa, and D. D. M. Wayner, Langmuir **15**, 3831 (1999).
[21] T. Yamada, T. Inoue, K. Yamada, N. Takano, T. Osaka, H. Harada, K. Nishiyama, and I. Taniguchi, J. Am. Chem. Soc. **125**, 8039 (2003).
[22] A. Fidélis, F. Ozanam, and J.-N. Chazalviel, Surf. Sci. **444**, L7 (2000).
[23] N. Y. Kim and P. E. Laibinis, J. Am. Chem. Soc. **120**, 4516 (1998).
[24] C. Gurtner, A. W. Wun, and M. Sailor, Angew. Chem., Int. Ed. **38**, 1966 (1999).
[25] M. R. Linford and C. E. D. Chidsey, Langmuir **18**, 6217 (2002).
[26] J. J. Boland and J. S. Villarrubia, Phys. Rev. B **41**, 9865 (1990).
[27] Y. Tanaka, K. Nishiyama, I. Taniguchi, T. Yamada, and T. Osaka (unpublished).
[28] D. Niwa, I. Inoue, H. Fukunaga, T. Akasaka, T. Yamda, T. Homma, and T. Osaka, Chem. Lett. **33**, 284 (2004).
[29] G. S. Higashi, Y. J. Chabal, G. W. Trucks, and K. Raghavachari, Appl. Phys. Lett. **56**, 656 (1990).
[30] S. Kaye and S. Tannenbaum, J. Org. Chem. **18**, 1750 (1953).
[31] I. A. Oxton, J. Mol. Struct. **56**, 57 (1979).
[32] C. J. Pouchert, The Aldrich Library of FT-IR Spectra Edition I; Aldrich Chemical Company, Inc.: Milwaukee, 1985.
[33] B. Schrader, *Raman/Infrared Atlas of Organic Compounds*, 2nd edition (VCH: Weinheim, NewYork, 1989).
[34] K. Hamaguchi, S. Machida, M. Nagao, F. Yasui, K. Mukai, Y. Yamashita, and J. Yoshinobu, J. Phys. Chem. B **105**, 3718 (2001).
[35] Y.-L. Chan, W.-W. Pai, and T. J. Chuang, J. Phys. Chem. B **108**, 815 (2004).
[36] G. Pelz, P. Mittler, K. M. T. Yamada, and G. Winnewisser, J. Mol. Spectrosc. **156**, 390 (1992).
[37] R. Roberge, C. Sandorfy, J. I. Matthews, and O. P. Strausz, J. Chem. Phys. **69**, 5105 (1978).
[38] R.-S. Zhai, Y.-L. Chan, P. Chuang, C.-K. Hsu, M. Mukherjee, T. J. Chuang, and R. Klauser, Langmuir **20**, 3623 (2004).
[39] E. Hirota, J. Mol. Spectrosc. **77**, 213 (1979).
[40] M. Wong, I. Ozier, and W. L. Meerts, J. Mol. Spectrosc. **102**, 89 (1983).
[41] A. Bondi, J. Phys. Chem. **68**, 441 (1964).
[42] M. A. Neumann, W. Press, C. Nöldeke, B. Asmussen, M. Prager, and R. M. Ibberson, J. Chem. Phys. **199**, 1586 (2003).
[43] S. Suto, R. Czajka, S. Szuba *et al.*, Acta Phys. Pol. A **104**, 289 (2003).
[44] Y. He, S. Bouzidi, B.-Y. Han, L.-M. Yu, P. A. Thiry, R. Caudano, and J.-M. Debever, Phys. Rev. B **54**, 17654 (1996).
[45] T. Miyadera, A. Koma, and T. Shimada, Surf. Sci. **526**, 177 (2003).
[46] S. Bouzidi, F. Coletti, J. M. Debever, P. A. Thiry, P. Dumas, and Y. J. Chabal, Phys. Rev. B **45**, 1187 (1992).
[47] S. Bouzidi, F. Coletti, J. M. Debever, P. A. Thiry, P. Dumas, and Y. J. Chabal, Surf. Sci. **269-270**, 829 (1992).

Downloaded 22 Aug 2012 to 131.215.16.11. Redistribution subject to AIP license or copyright; see http://jcp.aip.org/about/rights_and_permissions